PCCP

ROYAL SOCIETY OF CHEMISTRY

PAPER

Cite this: *Phys. Chem. Chem. Phys.*, 2024, **26**, 27382

Participation of transition metal atoms in noncovalent bonds†

Steve Scheiner

Received 26th September 2024,
Accepted 18th October 2024

DOI: 10.1039/d4cp03716b

rsc.li/pccp

The existence of halogen, chalcogen, pnicogen, and tetrel bonds as variants of noncovalent σ and π-hole bonds is now widely accepted, and many of their properties have been elucidated. The ability of the d-block transition metals to potentially act as Lewis acids in a similar capacity is examined systematically by DFT calculations. Metals examined span the entire range of the d-block from Group 3 to 12, and are selected from several rows of the periodic table. These atoms are placed in a variety of neutral MX_n molecules, with X = Cl and O, and paired with a NH_3 nucleophile. The resulting M···N bonds tend to be stronger than their p-block analogues, many of them with a substantial degree of covalency. The way in which the properties of these bonds is affected by the row and column of the periodic table from which the M atom is drawn, and the number and nature of ligands, is elucidated.

Introduction

The H-bond is arguably the most important of all noncovalent interactions, figuring prominently in a diverse range of chemical and biological phenomena such as solvation, genetic replication, and enzymatic activity.[1–8] Recent years have brought to the fore a class of closely related noncovalent bonds wherein the bridging proton is replaced by any of a large set of other atoms, mainly drawn from the right side of the periodic table.[9–17] Although these interactions do not have the advantage of a positive H atom to attract a nucleophile, they rely instead on a restricted region of positive electrostatic potential that lies along the extension of the covalent bond which connects this bridging atom to the Lewis acid molecule. This region of positive charge, attributed to a deficiency of electron density, has been termed a σ-hole[18,19] and thus the associated bonds are classified as σ-hole bonds. In a more general sense, there are situations where the positive region lies not along a bond axis, but rather above the plane of the molecule, and is thus referred to as a π-hole.[20–24]

It is common to subclassify these bonds according to the family of the periodic table from which the bridging atom is derived, thus leading to the halogen, chalcogen, pnicogen, tetrel, and triel bonds that have found their way into common chemical parlance. Their importance is undeniable, as their strength is comparable to the H-bond, exceeding it in many instances. Like the H-bond, these bonds too are major players in widespread chemical phenomena such as catalysis, supramolecular structure, self-assembly, and ion transport.[25–32] Intensive study of these interactions in recent years has led to a great deal of information and insights concerning their fundamental nature, their strength, and the way in which they are modified by both the identity of the bridging atom and any of its substituents.

There is of course no reason that these bridging atoms must be limited to the p-block elements on the right side of the periodic table. One might conjecture that the transition metals of the d-block, with their greater electropositivity, ought to present σ and π-holes that are even more positive than the non-metallic atoms to their right, and perhaps then stronger interactions with a nucleophile. And in fact, the recent literature has sprung to life with a rapidly increasing number of tentative observations of interactions that have all the markings of bonds of this sort. In the spirit of the p-block family, these bonds are often named after the particular column of the periodic table. Those involving Group 12 metals have been christened spodium bonds[33–40] and those including Group 11 go by the moniker of either regium or coinage metal bonds.[41–48] Osme bonds encompass Group 8,[49,50] matere bonds arise from Group 7,[51–55] wolfium bonds denote Group 6,[56,57] and erythronium bonds correspond to Group 5.[58]

Whereas a prodigious amount of work has been devoted to the p-block noncovalent bonds, which has yielded a solid understanding, analysis of their d-block analogues remains relatively scant. Most of the study to date has been centered on those particular systems that have been found in crystals. As such, previous work[33–58] has generally been devoted to one or a few isolated systems without a systematic variation of central atom and substituents. Moreover, this work has generally concerned itself with the particular geometry of the interaction within the context of the crystal. It therefore has

Department of Chemistry and Biochemistry, Utah State University, Logan, Utah 84322-0300, USA. E-mail: steve.scheiner@usu.edu

† Electronic supplementary information (ESI) available. See DOI: https://doi.org/10.1039/d4cp03716b

not identified the optimal distance or orientation of each sort of bond, nor has it elucidated the potential bond strength that might be achieved by geometry optimization in the absence of crystal packing forces that hold the two subunits in an arrangement that is less favorable than it might otherwise be.

There is thus a great deal left to learn about the interactions of these transition metal atoms. The work presented here attempts to remedy this deficiency and to begin the process of a systematic understanding of these σ and π-hole bonds that involve the transition metals. For this purpose, quantum chemical DFT calculations are brought to bear on a systematically varied set of systems. Transition metals considered span the entire range, from Group 3 to Group 12, and covering three different rows of the periodic table. Each metal atom M is covalently attached to a varying number n of substituents, MX_n. Both Cl and O are considered as substituents X, so as to encompass both single and double bonds. Calculations are not limited to singlets, but address higher multiplicities as well. For purposes of consistency, both internally and for comparison with other calculations in the literature, NH_3 is taken as the universal nucleophile to pair with each MX_n species. This Lewis base is strong enough to bring out the bonding properties of each acid, and small enough so as to avoid complicating secondary interactions. The calculations are limited to neutral systems, avoiding ions whose overall charge would greatly influence the bonding *via* what has been come to be called charge assistance.

The overall goal of this work is to elucidate the properties of these noncovalent bonds involving transition metal atoms as Lewis acids. How is the bonding affected by both the column and row of the metal atom? What is the effect of differing numbers and types of ligands? Another issue of prime concern is the geometry adopted by each sort of bond, and how this structure relates to the position of the σ or π-hole of the Lewis acid. As a subsidiary question, the work seeks to address how these d-block metal interactions compare with those of the p-block atoms. Also of interest is the classification of these bonds: are they noncovalent or covalent?

Methods

Quantum chemical calculations were performed *via* the density functional theory (DFT) formalism, within the context of the M06-2X functional[59] in conjunction with a polarized triple-ζ def2-TZVP basis set.[60,61] This basis set includes a relativistic pseudopotential on 4d and 5d transition metal atoms. This combination has been assessed and tested as highly accurate for interactions of the sort examined here.[62–69] The ultrafine integration grid applied here has been shown[70] to supply atomization energies to within 0.01 kcal mol^{-1}. The Gaussian 16[71] program was chosen as the specific means to conduct these computations. All geometries were fully optimized, and verified as true minima by the absence of imaginary vibrational frequencies. The convergence criteria for geometry optimizations were set to 0.00045 for the maximum force, 0.00300 for the RMS force, 0.0018 for the maximum displacement, and 0.0012 for the RMS displacement, all in a.u. SCF convergence criteria were 10^{-6} for both the maximum density matrix and the energy. Several benchmark calculations were performed at the CCSD level, also with the def2-TZVP basis.

Interaction energies were calculated as the difference between the energy of the entire complex, and that of the sum of the two constituent subunits within the geometry of the fully optimized dyad. The binding energy was defined in a similar manner but took as reference the optimized monomer geometries. Interaction energies were corrected for basis set superposition error *via* the standard Boys–Bernardi counterpoise protocol.[72,73] Zero-point vibrational energies were not added to these quantities.

Maxima in the molecular electrostatic potential (MEP) were measured on the 0.001 a.u. isodensity surface by the Multiwfn program[74] which was also used to elucidate electron localization function (ELF) diagrams. Atoms in Molecules (AIM) bond paths and their associated critical points[75] were located and their properties evaluated with the aid of AIMAll.[76] Wiberg bond indices[77–79] were evaluated with the NBO routines incorporated into Gaussian. The feasibility of applying a single configuration as the dominant one was tested *via* the T1 diagnostic.[80,81]

Results

The first section concerns itself with atoms drawn from the fourth period as a common feature. These atoms should be large enough to capture the full extent of noncovalent bonding of both p and d-block atoms. Secondly, they contain a small enough nuclear charge so as to minimize relativistic effects. Nonetheless, some of these effects are captured by the pseudopotentials introduced by the def2-TZVP basis set. Atoms from both lower and higher periods are discussed below in a later section.

Geometries and hole positions

The optimized structures of the complexes involving the p-block central atoms of Row 4 are pictured in Fig. 1 where it may be seen that they take on the classic geometries of halogen, chalcogen and pnicogen bonds for I, Te, and Sb, respectively, that have been well described in the literature. The NH_3 nucleophile is attracted to the σ-hole opposite the Cl–A bond in each case where A represents any of these central atoms. $SrCl_2$ is a linear monomer, which contains a circular band of positive MEP that surrounds the central Sr. The presence of the NH_3 causes the $SrCl_2$ unit to bend, as exhibited in Fig. 1(*g*).

The optimized geometries of the complexes containing an odd number of Cl ligands on a central M atom from the d-block are exhibited in Fig. 2. The structures generally fit with the idea of the NH_3 being attracted to a positive σ or π-hole above the M atom. As may be seen in Fig. S1 (ESI†), which collects the molecular electrostatic potential (MEP) of each monomer, the YCl_3 and $TcCl_3$ monomers are planar with a π-hole directly above the M. $AgCl_3$ is T-shaped and has a positive σ-hole directly opposite the equatorial Cl, attracting the NH_3 to constitute a square arrangement. $TcCl_5$ is square pyramidal, with a

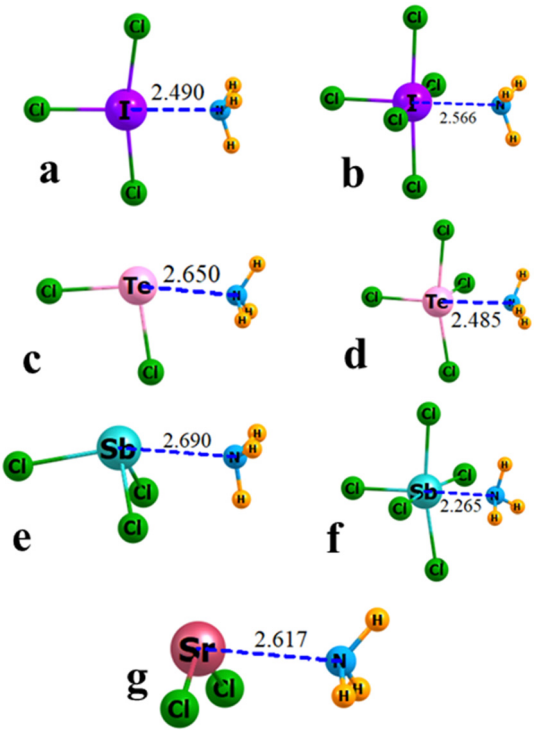

Fig. 1 Optimized geometries of complexes of NH_3 with (a) ICl_3, (b) ICl_5, (c) $TeCl_2$, (d) $TeCl_4$, (e) $SbCl_3$, (f) $SbCl_5$, and (g) $SrCl_2$. Distances in Å.

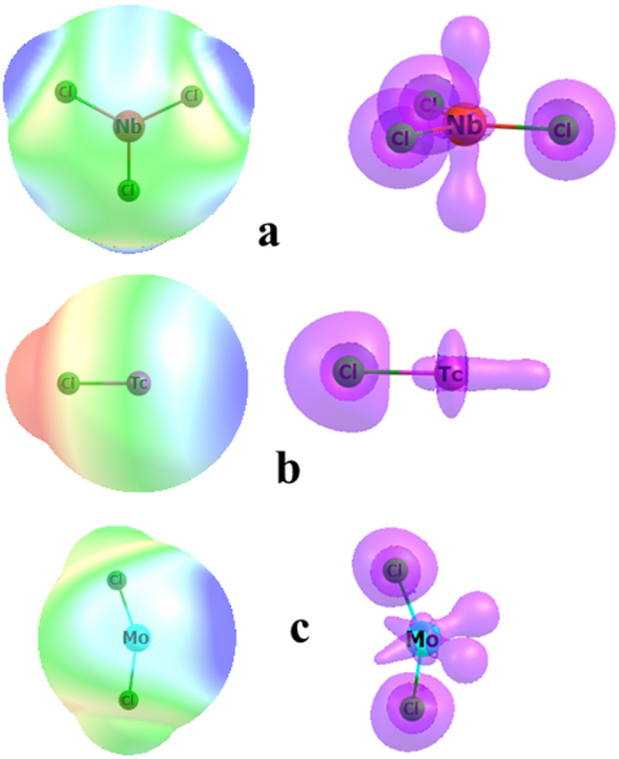

Fig. 3 Molecular electrostatic potential (left) and ELF (right) of (a) $NbCl_3$, (b) TcCl, (c) $MoCl_2$. MEP shows negative values in red, and positive in blue. ELF contour shown is 0.8 a.u.

σ-hole opposite the apical Cl. $NbCl_5$ is interesting in that its monomer geometry is trigonal bipyramid, and contains a σ-hole opposite each of the equatorial Cl atoms. However, the binding to NH_3 alters the structure to octahedral.

$NbCl_3$ is slightly different in some ways. Its π-hole above the Nb in its trigonal geometry, can be seen in Fig. 3(a) to shift away from the Nb vertical, toward the Cl–Nb–Cl bisector. This shift can be traced to the presence of an electron pair directly along this vertical, as depicted by the ELF diagram of Fig. 3(a). (ELF diagrams of all MCl_n monomers are contained in Fig. S2, ESI†). This pair is tantamount to a d_{z^2} orbital, which pushes the π-hole away from the vertical, also accounting for the bent shape of $NbCl_3\cdots NH_3$ in Fig. 2(b). Bending is also seen in $TcCl\cdots NH_3$ in Fig. 2(e), which is again attributable to the occupied ELF directly along the Cl–Tc axis on the right side of Fig. 3(b). This density displaces the σ-hole away from this axis so that the actual maxima lie some 36° off the axis, which accounts for the substantial nonlinearity in $TcCl\cdots NH_3$ in Fig. 2(e).

The structures of the MCl_n complexes with NH_3 for even values of n are displayed in Fig. 4. Again, with some exceptions, the NH_3 occupies a σ or π-hole of the central unit, which may be discerned from the MEPs in Fig. S3 (ESI†). Because of the presence of the ELF lobes perpendicular to the molecular plane of $MoCl_2$, displayed in Fig. 3(c), the position of the maximum in the MEP is displaced from the Cl–Mo–Cl axis by some 25°.

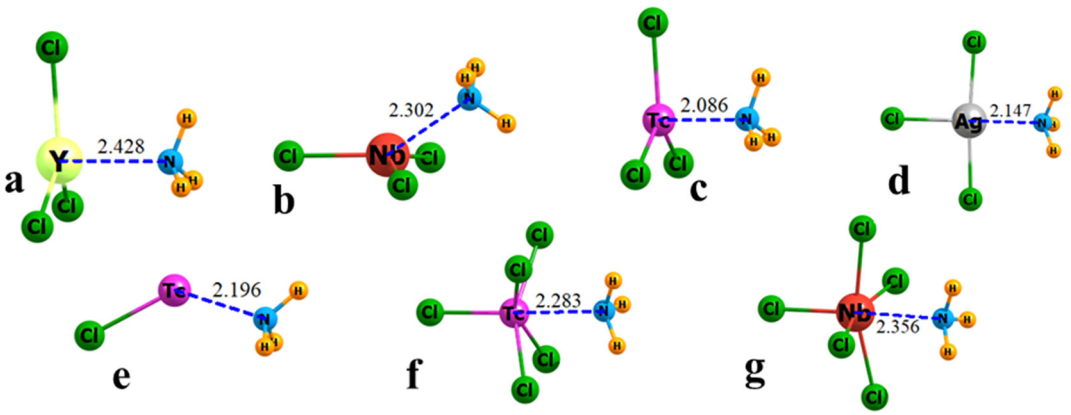

Fig. 2 Optimized geometries of complexes of NH_3 with (a) YCl_3, (b) $NbCl_3$, (c) $TcCl_3$, (d) $AgCl_3$, (e) TcCl, (f) $TcCl_5$, and (g) $NbCl_5$. Distances in Å.

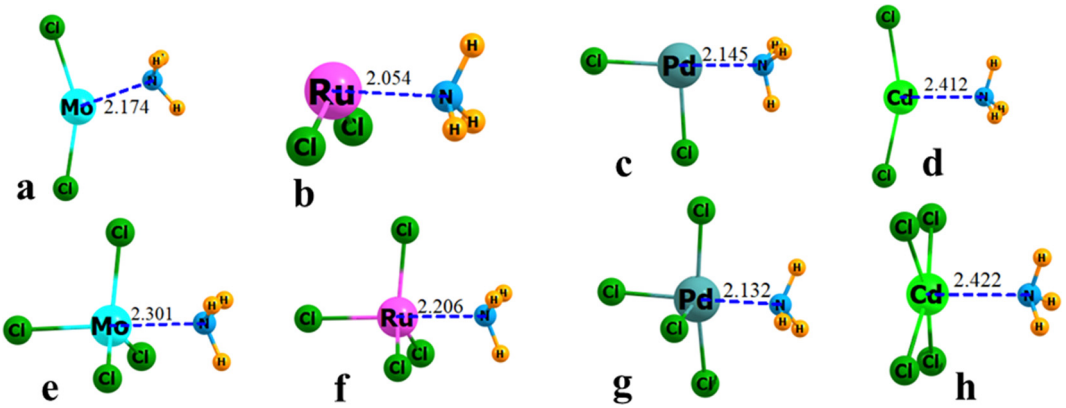

Fig. 4 Optimized geometries of complexes of NH_3 with (a) $MoCl_2$, (b) $RuCl_2$, (c) $PdCl_2$, (d) $CdCl_2$, (e) $MoCl_4$, (f) $RuCl_4$, (g) $PdCl_4$, and (h) $CdCl_4$. Distances in Å.

A similar displacement from the Cl–Pd–Cl midpoint axis of 41° occurs for $PdCl_2$. Of some interest, the interaction with NH_3 causes the linear geometry of $CdCl_2$ to bend. Otherwise, these MCl_n monomers largely retain their overall shape when engaged in the complex.

Energetics and bondlengths

The energetics of formation of the various complexes are collected in Table 1, along with other key aspects of the complexes. The interaction energy E_{int} reflects the difference between the energy of the complex and the sum of the two subunits, both within the geometry they take on within the dyad. In the case that the energies of the monomers reflect their fully optimized geometries, the energy difference E_b is defined as the binding energy, which is also the energy of the complexation reaction. These two quantities differ by the deformation energy E_{def} required to transform the monomer geometries into their dyad structures. In most cases in Table 1, this deformation energy is rather small and E_b is nearly equal to E_{int}. But there are several cases where there is a significant difference. One such example is $NbCl_5$, where the trigonal bipyramidal monomer is transformed into a square pyramid so as to accommodate the NH_3 within an overall octahedral framework. Other parameters contained in Table 1 include V_{max}, the maximum of the MEP on the 0.001 a.u. isodensity surface of the monomer, which represents a measure of the depth of the σ or π-hole. The next two columns of Table 1 compare the distance from the central atom to the incoming N of NH_3, or to the Cl atoms which surround it.

Focusing first on the p-block atoms in the upper portion of Table 1, the interaction energies cover a varied range, between 13 and 36 kcal mol^{-1}. There is no set relationship between E_{int} and the number of Cl ligands. The halogen bonds to I are strongest for n = 3, whereas the pnicogen bonds to Sb are weakest for n = 3. The pnicogen bonds appear to be the strongest in general, at least for n = 1 or 5, followed by the tetrel bonds to Sn and the bond involving Sr. The relation between E_{int} and V_{max} is not very robust. For example, the σ-hole depth of the $SbCl_3$ and $SbCl_5$ monomers are 40.9 and 23.6 kcal mol^{-1}, respectively, but E_{int} to the latter is nearly three times the magnitude of the former. On the other hand, there is a modest correlation with R^2 = 0.61 between the interaction energy and R_N, in that the shortest bonds tend to be the strongest, but this correlation is not without exceptions.

The next section of Table 1 provides similar data for the interactions between NH_3 and the d-block elements, again with varying numbers of Cl ligands on each. In a general overview,

Table 1 Energetic (kcal mol^{-1}) and geometric (R in Å) aspects of $ACl_n\cdots NH_3$ complexes

Group	A	n	$-E_{int}$	$-E_b$	V_{max}	R_N	R_{Cl}[a]	d_N	d_{Cl}
p-Block									
17	I	1	12.91	13.28	46.3	2.625	2.375	1.29	1.02
		3	20.24	18.32	49.3	2.490	2.440	1.22	1.05
		5	18.44	16.24	42.0	2.315	2.423	1.13	1.04
16	Te	2	13.22	13.29	43.9	2.650	2.364	1.28	1.01
		4	21.03	18.41	46.4	2.485	2.400	1.20	1.02
15	Sb	1	31.28	31.27	62.0	2.318	2.422	1.10	1.01
		3	13.21	13.18	40.9	2.690	2.367	1.27	0.99
		5	36.32	29.45	23.6	2.265	2.351	1.07	0.98
14	Sn	2	24.67	24.63	51.9	2.399	2.431	1.14	1.02
		4	26.93	18.84	35.1	2.358	2.336	1.12	0.98
2	Sr	2	24.78	25.30	126.4	2.617	2.648	1.02	0.93
d-Block									
3	Y	1	25.12	25.55	13.7	2.455	2.440	1.05	0.93
		3	38.60	39.01	161.0	2.428	2.475	1.04	0.94
5	Nb	1	42.88	42.98	120.7	2.261	2.283	1.04	0.93
		3	34.45	27.80	18.3	2.302	2.294	1.06	0.93
		5	35.07	29.38	20.2	2.356	2.321	1.08	0.94
6	Mo	2	37.52	37.28	15.6	2.174	2.279	1.04	0.96
		4	32.47	30.20	27.1	2.301	2.262	1.10	0.95
7	Tc	1	40.38	41.91	91.8	2.196	2.234	1.10	0.98
		3	55.64	54.40	19.3	2.086	2.241	1.05	0.99
		5	31.95	23.22	20.4	2.283	2.262	1.15	1.00
8	Ru	2	55.37	54.16	23.5	2.054	2.246	1.05	1.00
		4	31.77	27.53	20.0	2.206	2.207	1.13	0.99
10	Pd	2	37.72	38.03	70.7	2.145	2.237	1.12	1.02
		4	40.18	40.15	53.4	2.132	2.255	1.12	1.03
11	Ag	1	28.90	30.06	74.3	2.246	2.328	1.13	1.03
		3	39.58	40.01	58.8	2.147	2.292	1.08	1.01
12	Cd	2	22.76	20.92	51.4	2.412	2.351	1.17	1.00
		4	23.38	22.75	57.3	2.422	2.390	1.17	1.02

[a] Average of all A–Cl.

these interactions appear to be stronger than those of the p-block. In brief, the p-block binding energies range from 13 to 31 kcal mol^{-1}, while the corresponding values for the d-block are 21 to 54 kcal mol^{-1}. The energetics depend on the number of Cl ligands, but there is no clear rule relating these two parameters. For example the binding energy of YCl_3 is nearly double that of YCl, whereas NbCl has a much larger binding energy than either $NbCl_3$ or $NbCl_5$. Tc alters either of those patterns wherein the E_b ordering is $TcCl_3 > TcCl > TcCl_5$. There is also inconsistent ordering for even n, as for example $RuCl_2 > RuCl_4$ but $PdCl_2 < PdCl_4$.

The depth of the σ or π-hole is typically a reasonably reliable indicator of the strength of noncovalent bonds such as halogen, chalcogen, *etc.* But V_{max}, the maximum of the MEP on the 0.001 a.u. isodensity surface of the central atom, does not fulfill this role very well in these cases. In the Sb pnicogen bonds, for instance, V_{max} of SbCl is nearly three times the magnitude for $SbCl_5$, but their binding energies with NH_3 are very similar. An even more extreme illustration is YCl_n. V_{max} of YCl_3 is more than an order of magnitude larger than for YCl, but is bound only slightly more strongly. As well, even though TcCl has a V_{max} four times larger than $TcCl_3$, it is nevertheless more weakly bound.

The weak connection between binding strength and V_{max} is an indicator that these bonds are perhaps more similar to covalent than to noncovalent. One way in which to view this question is through the window of bond lengths. The next two columns of Table 1 report the bondlengths of the central atom to the *N* of NH_3 is compared to the A–Cl bondlengths in each complex. It must first be stated at the outset that the Cl atom is somewhat larger than *N*, with a 0.28 Å longer covalent bond radius.[82] As another issue, each of the central atoms has a different radius, further complicating direct comparisons from one complex to the next. In an effort to facilitate the appropriate comparisons, each bondlength was normalized by dividing it by the sum of the two relevant covalent bond radii. So $d_N = R_N/(r_{cov,N} + r_{cov,A})$, with a similar definition for d_{Cl}.

These normalized quantities are listed in the final two columns of Table 1 from which it may be seen that d_{Cl} is right at or very close to unity, suggesting the A–Cl bonds have standard covalent character. The largest deviation is a value of 1.05 for the halogen-bonded $ICl_3\cdots NH_3$. The d_N values are significantly larger than d_{Cl}. The smallest d_N of 1.02 occurs for $SrCl_2$, but this value is still significantly larger than 0.93 for d_{Cl} in the same system. Some of the p-block complexes contain the largest values of d_N; notably the halogen-bonded ICl and ICl_3, and the pnicogen bond involving $SbCl_3$, with values exceeding 1.2. These systems would thus be thought of having the smallest component of covalent bonding. This normalized d_N parameter lies generally in the vicinity of 1.1, which might lead to the conclusion of a significant degree of covalency.

Table 2 AIM properties of bond critical points and Wiberg Bond Index (WBI) of $ACl_n\cdots NH_3$ complexes, all in a.u.

			ρ		V		H		WBI	
Group	A	*n*	A···N	A···Cl	A···N	A···Cl	A···N	A···Cl	A···N	A···Cl
p-Block										
17	I	1	0.0379	0.0921	−0.0299	−0.0897	−0.0041	−0.0369	0.166	0.821
		3	0.0550	0.0864	−0.0437	−0.0783	−0.0112	−0.0319	0.230	0.644
		5	0.0516	0.0936	−0.0377	−0.0842	−0.0087	−0.0543	0.191	0.630
16	Te	2	0.0357	0.0910	−0.0270	−0.0955	−0.0044	−0.0363	0.160	0.814
		4	0.0537	0.0858	−0.0426	−0.0902	−0.0125	−0.0375	0.239	0.701
15	Sb	1	0.0615	0.0747	−0.0657	−0.0791	−0.0130	−0.0228	0.394	0.732
		3	0.0326	0.0863	−0.0230	−0.0958	−0.0038	−0.0317	0.147	0.747
		5	0.0746	0.0930	−0.0803	−0.1020	−0.0218	−0.0369	0.338	0.699
14	Sn	2	0.0515	0.0710	−0.0511	−0.0786	−0.0084	−0.0192	0.274	0.616
		4	0.0572	0.0878	−0.0601	−0.1054	−0.0111	−0.0295	0.269	0.728
2	Sr	2	0.0318	0.0433	−0.0271	−0.0430	0.0010	−0.0020	0.062	0.177
d-Block										
3	Y	1	0.0500	0.0734	−0.0478	−0.0832	−0.0055	−0.0171	0.150	0.632
		3	0.0503	0.0652	−0.0481	−0.0733	−0.0047	−0.0120	0.273	0.848
5	Nb	1	0.0781	0.1066	−0.0841	−0.1328	−0.0182	−0.0407	0.301	1.021
		3	0.0669	0.1016	−0.0722	−0.1239	−0.0126	−0.0377	0.427	1.313
		5	0.0634	0.1009	−0.0618	−0.1197	−0.0121	−0.0378	0.453	1.250
6	Mo	2	0.0833	0.1008	−0.1107	−0.1324	−0.0174	−0.0394	0.505	1.105
		4	0.0638	0.1064	−0.0775	−0.1362	−0.0095	−0.0403	0.440	1.293
7	Tc	1	0.0781	0.1181	−0.0943	−0.1475	−0.0155	−0.0461	0.361	1.041
		3	0.0978	0.1066	−0.1548	−0.1410	−0.0215	−0.0370	0.646	1.141
		5	0.0721	0.1109	−0.0712	−0.1327	−0.0137	−0.0415	0.485	1.185
8	Ru	2	0.1041	0.1035	−0.1622	−0.1347	−0.0245	−0.0335	0.586	0.973
		4	0.0743	0.1192	−0.1023	−0.1478	−0.0113	−0.0454	0.457	1.156
10	Pd	2	0.0801	0.1036	−0.1159	−0.1250	−0.0122	−0.0315	0.334	0.835
		4	0.0881	0.1029	−0.1181	−0.1132	−0.0165	−0.0317	0.433	0.844
11	Ag	1	0.0652	0.0807	−0.0862	−0.1012	−0.0078	−0.0181	0.209	0.555
		3	0.0840	0.0912	−0.1099	−0.1006	−0.0142	−0.0240	0.356	0.674
12	Cd	2	0.0466	0.0770	−0.0534	−0.0968	−0.0045	−0.0170	0.169	0.595
		4	0.0457	0.0700	−0.0524	−0.0742	−0.0044	−0.0146	0.208	0.516

Electron density topology

Of course, bondlength is not the only measure of the strength as a bond, shown for example by Kaupp *et al.*[83] in their studies of the Sn–Sn bond. It is therefore necessary to examine other means of assessing these bonds. Analysis of the electron density offers another perspective on the strengths of the various bonds.[75] AIM finds a clear bond path from the central A atom to N and to each of the Cl ligands in these complexes. Three of the prime characteristics of the bond critical points are compiled in Table 2. The first of these is the density at the bond critical point, ρ. The density of the A···N bond in the first column is somewhat smaller than for the A–Cl bonds. The former range from 0.032 up to 0.104 a.u. The lower end of this spectrum would be best classified as noncovalent while the higher values are clearly in the covalent domain.[75,84] In most cases, ρ is larger for the A–Cl bond, but the ratio between these two quantities is quite variable. In some complexes this ratio is substantial as in the halogen bonded $ICl\cdots NH_3$, where the ICl density is 2.4 times larger than I···N. But in others like $RuCl_2\cdots NH_3$ the two densities are much closer to one another.

There is some sentiment in the literature to evaluate bond energies *via* a linear relationship with the potential energy density V at the bond critical point.[85,86] The values of V in the next two columns of Table 2 are consistent with the ρ patterns in that in most cases –V for the A–N bond is smaller than that of the A–Cl bond. In fact, both ρ and V for the A–N bond correlate nicely with the interaction energy, as is evident in Fig. 5, where the R^2 correlation coefficients are 0.81 and 0.89, respectively. The usefulness of these correlations is exemplified in that the interaction energy is nearly precisely equal to the bond critical point density when expressed in the same units: $E_{int} = -1.00\ \rho$. The relationship with the potential energy density comes to $E_{int} = 0.54$ V, similar to equations occasionally used for H-bonds.[87,88] This consistency is notable in light of the diversity of different sorts of central A atoms under consideration here.

The sign of the total energy density H is commonly thought to differentiate between a covalent and noncovalent bond.[84] Nearly all of these H quantities in the next two columns of Table 2 are negative, which suggests a significant covalent contribution. Importantly, H is consistently considerably more negative for the A–Cl bonds as compared to A–N. The ratio of the former to the latter is generally between 2 and 9, so H indicates the A–N bonds to be significantly weaker than A–Cl.

Another measure of bond strength is the Wiberg bond index (WBI),[77–79] which is listed in the last two columns of Table 2. With regard to the p-block atoms in the upper section of the table, the WBI of the A–Cl bonds are short of unity, generally around 0.6–0.7. But the WBI of the A···N interactions are much smaller, all below 0.4, which would argue for these bonds being primarily noncovalent. The bond strengths of both varieties in the $SrCl_2\cdots NH_3$ complex are much weaker, commensurate with the other AIM markers in the table.

Turning next to the d-block atoms, the WBI of the A–Cl bonds are generally close to or above unity, although they tail off a bit for Y, Ag, Cd. But again, these same quantities are considerably smaller for the A···N interactions, by a factor of 2 to 4. Nonetheless, the WBI of most of the A–N bonds exceed 0.4. The metal atoms for which this threshold is not attained are again the metals Y, Ag, and Cd which seem to engage in weaker bonds of both types. This pattern is true of the other AIM markers in Table 2.

Size dependence

The results presented to this point have been limited to the 4d transition metals. It is of interest to examine how the results might change by the consideration of either lighter or heavier atoms from each column. For this purpose, all atoms from Groups 6, 8, 10, and 12 were examined, from 3d to 5d, for both MCl_2 and MCl_4 cases, and compared with one another. The relevant results are reported in Table 3 which compile

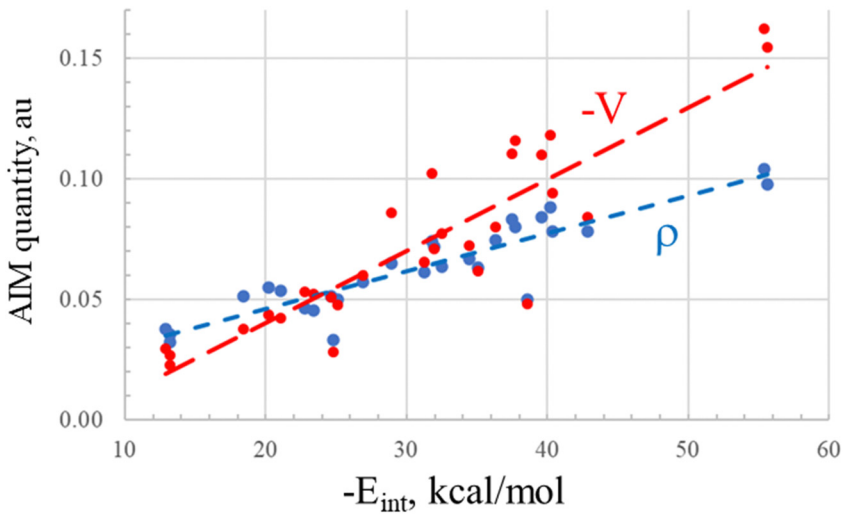

Fig. 5 Relationship between indicated AIM quantities and interaction energies.

Table 3 Energetic (kcal mol^{-1}) geometric (Å), and AIM (a.u.) data for $ACl_n\cdots NH_3$ complexes with A taken from rows 3–5 of the periodic table

Group		n	$-E_{int}$	$-E_b$	V_{max}	R_N	R_{Cl}[a]	ρ_N	ρ_{Cl}
6	Cr	2	37.55	36.32	30.7	2.089	2.235	0.0712	0.0882
		4[b]	30.05	24.90	15.5	2.171	2.149	0.0649	0.1060
	Mo	2	37.52	37.28	15.6	2.174	2.279	0.0833	0.1008
		4	32.47	30.20	27.1	2.301	2.262	0.0638	0.1064
	W	2	50.43	50.24	22.5	2.200	2.270	0.1311	0.1602
		4	26.58	18.32	20.0	2.294	2.284	0.1103	0.1566
8	Fe	2	50.26	49.11	26.6	2.003	2.177	0.0800	0.0904
		4	30.06	19.61	13.2	2.087	2.123	0.0752	0.1071
	Ru	2	55.37	54.16	53.4	2.132	2.207	0.1041	0.1035
		4	31.77	27.53	74.3	2.246	2.328	0.0743	0.1192
	Os	2	50.89	47.01	2.2	2.037	2.256	0.1204	0.1135
		4	35.34	31.48	25.2	2.205	2.333	0.0824	0.1238
10	Ni	2	54.21	51.49	69.3	1.935	2.152	0.0984	0.0877
		4	40.15	37.51	34.8	1.989	2.152	0.0917	0.0954
	Pd	2	37.72	38.03	70.7	2.145	2.237	0.0801	0.1036
		4	40.18	40.15	53.4	2.132	2.256	0.0881	0.1029
	Pt	2	42.92	42.52	53.2	2.109	2.226	0.1011	0.1227
		4	46.57	46.15	55.3	2.112	2.262	0.1060	0.1183
12	Zn	2	30.70	26.12	48.0	2.139	2.174	0.0620	0.0837
		4	32.34	—	—	2.137	2.288	0.0626	0.0640
	Cd	2	22.76	20.92	51.4	2.412	2.351	0.0466	0.0770
		4	23.38	22.75	57.3	2.422	2.390	0.0457	0.0700
	Hg	2	12.28	12.08	36.8	2.654	2.313	0.0340	0.1015
		4	15.12	15.63	44.8	2.615	2.330	0.0367	1.1005

[a] Average of all A–Cl. [b] One imaginary frequency.

rows 3–5 together, from top to bottom for each group. In most cases, the atoms both above and below those from period 4 take on the same shape as the $ACl_n\cdots NH_3$ dyads in Fig. 2 and 4. There are two exceptions, pictured in Fig. S4 (ESI†). Unlike the $RuCl_2$ dyad where the NH_3 approaches perpendicular to the acid, the replacement of Ru by Fe places the NH_3 in the $FeCl_2$ molecular plane. The MEP and ELF diagrams of the two MCl_2 monomers are quite similar, as is evident in Fig. S4 (ESI†). The second change occurs when Pd of $PdCl_2$ is replaced by its lighter congener Ni. Rather than approach the metal along a Cl–M bond extension as in the former case, the N lies directly along the Cl–Ni–Cl bisector in the latter. Again, Fig. S4 (ESI†) stresses the similarity of the MEP and ELF structures surrounding the two MCl_2 monomers.

Beginning with Group 6, the MCl_2 interactions with NH_3 are strongest for W, with Cr and Mo very similar to one another. Adding two more Cl ligands tends to weaken the interaction, particularly for W. The trends are different for Group 8. The MCl_2 species form the strongest bonds with NH_3, with E_{int} exceeding 50 kcal mol^{-1}, largest for Ru. While still strong, the MCl_4 species form somewhat weaker bonds, just above 30 kcal mol^{-1}, with gradual growth as the M atom becomes heavier.

Group 10 exhibits some different trends. While $NiCl_2$ is particularly strongly bound, the Pd and Pt analogues are somewhat weaker in this regard, although still around 40 kcal mol^{-1}. While the addition of two more Cl ligands weakens the Ni$\cdots$N bond, it has the opposite effect for Pd and Pt which both show an increase. The complexes involving Group 12 are among the weakest. The $ZnCl_2\cdots NH_3$ interaction energy is 30.7 kcal mol^{-1} but drops quickly as the atom grows larger, down to only 12.3 kcal mol^{-1} for $HgCl_2$. Adding two more Cl ligands has only a minor effect. $ZnCl_4$ presents an interesting situation in that the monomer spontaneously dissociates to $ZnCl_2$ + Cl_2, although it remains intact when interacting with NH_3.

As in many of the fourth period cases discussed above, the depth of the σ or π-hole appears to generally have little influence upon the strength of the ultimate M$\cdots$N bond. For example, even though V_{max} for $OsCl_2$ is only equal to 2.2 kcal mol^{-1}, this species nonetheless forms one of the strongest bonds to NH_3. On the opposite extreme, the fairly large V_{max} of 44.8 kcal mol^{-1} for $HgCl_4$ results in only a small interaction energy. Unlike V_{max}, the M$\cdots$N critical point density in the penultimate column of Table 3 is modestly correlated with the interaction energy for this entire set, with R^2 = 0.67.

The MEPs of the various monomers are all presented in Fig. S6 and S7 (ESI†), which can be compared with the systems described above.

Higher multiplets

The closeness in energy of the d-orbitals with themselves and others leads to the possibility that the singlet is not necessarily the state of lowest energy. It is quite reasonable to suppose that states higher in multiplicity may very well be comparable or lower in energy. It is thus worthwhile to consider how the data and trends discussed above might be altered for such higher-multiplicity states. For a number of the ACl_n monomers, it was indeed found that the triplet or even the quintuplet state was more stable than the singlet. These cases are displayed in Table 4 where E_{rel} refers to the energy of the optimized geometry of this particular state of the monomer in comparison to the singlet. It is clear that some of these higher multiplets are indeed substantially lower in energy, some by more than 40 kcal mol^{-1}.

The energetic and other characteristics of the complexes formed by each such species with NH_3 are listed in the remaining columns of Table 4. The triplet or quintuplet states of NbCl form a slightly weaker complex than does the singlet. The similarity of the triplet and quintuplet binding energies occurs despite their vastly different values of V_{max}. On the other hand, there is a reversal for $NbCl_3$ where the triplet is slightly more strongly bound than the singlet. Raising the multiplicity

Table 4 Characteristics of multiplet states of ACl_n. Energies and V_{max} in kcal mol^{-1}, R in Å

Group	A	n	$2S+1$	E_{rel}[a]	$-E_{int}$	$-E_b$	V_{max}	R_N	R_{Cl}
5	Nb	1	3	−25.48	36.39	37.11	16.8	2.260	2.287
			5	−33.77	35.14	35.75	110.2	2.333	2.361
		3	3	−11.39[a]	36.20	33.22	26.7	2.270	2.295
6	Mo	2	3	−23.16	35.12	33.93	24.9	2.208	2.297
			5	−45.72	36.82	36.12	38.9	2.249	2.344
		4	3	−25.97	33.45	29.06	27.9	2.298	2.270
7	Tc	1	3	−31.34	42.73	44.12	100.5	2.299	2.257
			5	−55.82	37.92	39.15	78.9	2.246	2.289
		3	3	−26.55	43.22	30.13	12.5	2.081	2.287
			5	−41.82	39.95	37.29	50.4	2.236	2.300
		5	5	−3.86	39.88	38.62	56.1	2.225	2.347
8	Ru	2	3	−25.84	46.31	36.75	43.3	2.179	2.263
10	Pd	2	3	−4.01	30.58	25.64	23.5	2.275	2.287
12	Cd	4	3	−1.59	26.28	24.77	58.3	2.380	2.455

[a] Relative to singlet.

of $MoCl_n$ does little to change its binding energy for either n = 2 or 4. The Tc atom has the largest diversity of stable higher multiplets. The binding of TcCl is not much affected by higher multiplicity, whereas that of $TcCl_3$ is weakened a bit for either the triplet or quintuplet. $TcCl_5$, on the other hand, binds more tightly in its quintuplet than singlet state.

The atoms of Groups 8–12 all have a triplet state available, in addition to the singlet. The former state of $RuCl_2$ is slightly weakened compared to the latter, but remains quite tightly bonded to NH_3, by some 40 kcal mol^{-1}. The same is true of $PdCl_2$, whereas the triplet state of $CdCl_4$ is somewhat more strongly bonded than is its singlet. Overall, the consideration of higher-order spin states strengthens some of the bonds and weakens others. But these changes are relatively minor, and do little to change the general patterns.

Particularly in the case of transition metals with their partially filled d-shells, there is always a question at to how well a single configuration can deal with a particular electronic state. An answer to this question arises in the context of the T1 diagnostic that was developed by Lee and Taylor.[80] The values of this parameter are listed in Table S1 (ESI†) for all of the systems considered here, both p and d-block atoms, and with variable numbers of Cl ligands. The values of T1 are all comfortably below the 0.05 that has been proposed as an important threshold[89,90] to gauge the applicability of the single configuration prescription. The sole exception is the triplet state of NbCl where T1 reaches up to 0.22, while all others are below 0.04, and some much smaller. Other authors have proposed somewhat differing T1 thresholds, for example, 0.05[90] for 3d metals, and 0.045 for 4d metals.[91] In any case, the T1 metric is not fully reliable in all cases,[92,93] and others have been proposed[90,91,94] as supplementary tests.

Oxygen ligands

It would be instructive to examine how ligands other than Cl might play out in terms of the various sorts of interactions under consideration. For this purpose, 2, 3, and 4 O atoms were placed around several of the central metal atoms, and a NH_3 then allowed to approach. For illustrative purposes, Mo, Ru, and Pd were taken as representative of Groups 6, 8, and 10.

The resulting optimized complexes are exhibited in Fig. 6 for Mo, Ru, and Pd. As depicted in Fig. 6, the various MO_2 monomers are bent. NH_3 approaches MoO_2 and RuO_2 along the bisector, but leaves the molecular plane for PdO_2. Whereas MoO_3 is pyramidal, both RuO_3 and PdO_3 are planar. While the latter retains is planarity in its complex with NH_3, the other two MO_3 complexes are clearly pyramidal. RuO_4 and PdO_4 are tetrahedral, and NH_3 approaches along the extension of a O–M axis, coincident with a σ-hole. In contrast, MoO_4 was not found to be a stable species, dissociating spontaneously to $MoO_2 + O_2$. Of some interest, there is a second minimum found for the $RuO_3\cdots NH_3$ complex. The structure in Fig. 6(e) differs from 6d in having a much longer Ru···N distance, 3.22 *vs.* 2.06 Å. As explained below, this outer-sphere complex is less stable than the shorter one.

The salient characteristics of these complexes are reported in Table 5. Those involving Mo are particularly strong, with interaction energies of 47 and 59 kcal mol^{-1} for n = 2 and 3, respectively. PdO_2 and PdO_3 are quite strong as well, around 40 kcal mol^{-1}. This interaction energy drops down to 26 kcal mol^{-1} for n = 4. The bond strength diminishes along with n for the Ru series, from 35 kcal mol^{-1} for RuO_2 down to 8 kcal mol^{-1} for RuO_4. The pair of minima for RuO_3 are interesting in a number of respects. Although the inner-sphere complex has a far higher interaction energy, its binding energy is much reduced, due a large deformation energy of 15 kcal mol^{-1} when attached to NH_3. Much of this destabilization is due to the pyramidalization that contrasts with its optimized planar geometry. The sum of the three O–Mo–O angles in the complex differs from 360° by 15°. Also contributing is the stretching within the three Ru–O bonds by as much as 0.13 Å.

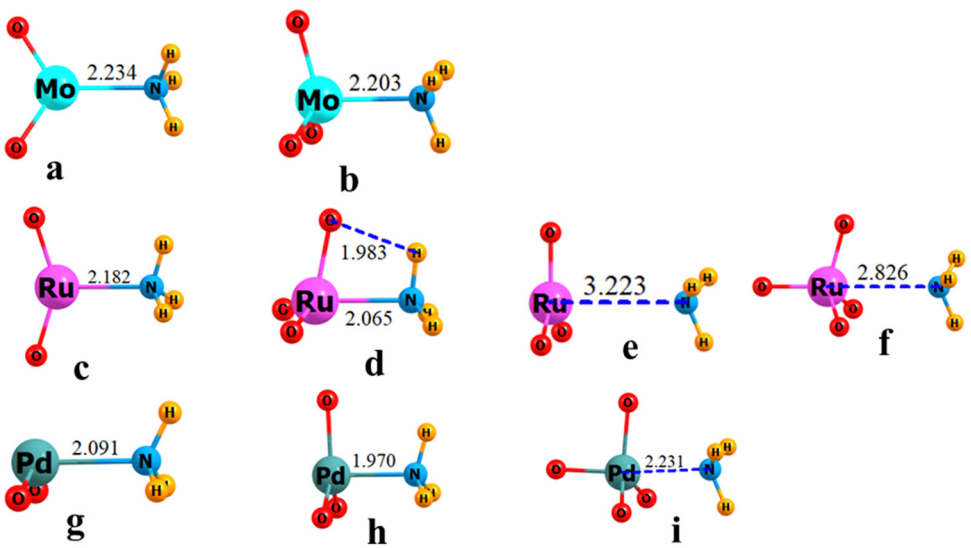

Fig. 6 Optimized geometries of complexes of NH_3 with (a) MoO_2, (b) MoO_3, (c) RuO_2, (d) RuO_3, (e) RuO_3 (second minimum), (f) RuO_4, (g) PdO_2, (h) PdO_3 and (i) PdO_4. Distances in Å.

Table 5 Properties of $AO_n\cdots NH_3$ complexes, E and V in kcal mol^{-1}, R in Å, ρ in a.u.

Group	A	n	$-E_{int}$	$-E_b$	V_{max}	R_N	R_O	ρ_N	ρ_O
6	Mo	2	47.30	45.93	63.4	2.234	1.687	0.0794	0.2754
		3	58.56	59.15	189.4	2.203	1.699	0.0825	0.2683
8	Ru	2	35.35	35.28	48.1	2.182	1.659	0.0839	0.2896
		3	23.39	8.04	20.8[a]	2.065	1.695	0.1119	0.2722
		3[b]	3.50	4.16	20.8[a]	3.223	1.655	0.0135	0.2971
		4	8.34	7.25	31.9	2.826	1.654	0.0210	0.3350
10	Pd	2	37.32	34.94	26.0	2.091	1.745	0.0973	0.3335
		3	40.85	31.67	33.3	1.970	1.754	0.1346	0.2215
		4	25.84	15.79	27.6	2.231	1.746	0.0717	0.2361

[a] Above O···O. [b] Secondary minimum.

Whether inner or outer-shell complex, the binding energy within $RuO_3\cdots NH_3$ is fairly small, much less than 10 kcal mol^{-1}.

With the exception of RuO_4, the R_N distances are fairly short, consistent with covalency. This categorization is reinforced by their large BCP densities, well exceeding 0.07 a.u. It would appear then that such strong bonding is the rule in these cases, with RuO_4 as the exception. As reported in Table S2 (ESI†), these singlet states are fairly well represented by a single electron configuration, with T1 tests generally below 0.05.

In terms of a comparison of the O with Cl ligands, it must first be stressed that the latter engage in single bonds with the central M, while O tends toward shorter double bonding. Starting with the matere bonds involving Mo, there is significant strengthening of M···N upon the replacement of Cl with O. The interaction energies in the 32–38 kcal mol^{-1} range for $MoCl_2$ and $MoCl_4$ are raised up to around 50 kcal mol^{-1} for MoO_2 and MoO_3. The overall structure of the MoX_2 complex is altered a bit by the Cl → O mutation, moving the NH_3 down to the O–Mo–O bisector, as is seen in Fig. 6(a), guided in part by the high electron densities of the ELF diagram in Fig S5a (ESI†). (ELF diagrams for all MO_n monomers are contained in Fig. S5, ESI†).

A similar displacement of NH_3 to the O–Ru–O bisector occurs for RuO_2 in Fig. 6(c). What would appear to be a weak NH···O H-bond in Fig. 6(d) rotates the RuO_3 C_3 axis. (This H-bond is confirmed by NBO by way of a $O_{lp} \rightarrow \sigma^*(NH)$ second-order perturbation energy E_2 of 6.2 kcal mol^{-1}, although AIM does not find a bond path connecting these two atoms.) However, the secondary minimum in Fig. 6(e) has no such perturbing interaction, and the RuO_3 retains its planar shape within a C_{3v} dyad. The Cl → O replacement does little to alter the shape of the RuX_4 complex with NH_3, as witness the similarity between Fig. 6(f) and 4(f). The bond energy to Ru is more dependent upon the number of Cl ligands, 55 and 32 kcal mol^{-1} for n = 2 and 4, respectively. Mutating the Cl ligands to O significantly reduces these interaction energies. All are less than 40 kcal mol^{-1}, and some less than 10.

Unlike the previous two sets, the replacement of Cl by O has only a very small effect on the Pd···N interaction energy which hovers around 40 kcal mol^{-1}. The exception is PdO_4 where this quantity drops off to 26 kcal mol^{-1}. This replacement alters the basic shape of the PdX_2 complex. Rather than adopting a position directly along a Cl–Pd extension as in Fig. 4(c), the NH_3 moves out of the PdO_2 molecular plane so as to form a trigonal pyramid around the central Pd in Fig. 6(g). Another shape change occurs for PdX_4. The complex in Fig. 4(g) consists of trigonal bipyramid with NH_3 occupying an equatorial position, directly opposite one of the other equatorial Cl centers. One could describe that in Fig. 6(i) in a similar way but with the NH_3 moved to an axial site. But perhaps a more accurate picture would place the PdO_4 in a tetrahedral structure, with NH_3 lying along a O–Pd bond extension, not too different from the $RuO_4\cdots NH_3$ complex in Fig. 6(f).

With respect to the AIM assessment of the M···N bond strengths the ρ_N quantities in Table 5 are suggestive of a high degree of covalency in most cases, with BCP densities exceeding 0.07 a.u. In that respect, the Cl → O mutation would seem to strengthen these bonds. There are two exceptions, both involving Ru. This density is only 0.021 a.u. for the complex with RuO_4. While the Ru–N bond is clearly covalent for the more stable of the two complexes with RuO_3, the higher-energy dyad falls clearly into the noncovalent range with ρ only 0.0135 a.u., and with a Ru···N separation of 3.223 Å.

The MEPs of the relevant MOn monomers are provided in Fig. S8 (ESI†).

Discussion

The interactions between the various d-block metals and a NH_3 nucleophile tend to be stronger and shorter than the standard noncovalent bonds of the halogen, chalcogen, pnicogen, and tetrel types. The interaction and binding energies of the latter show some variability with the number of Cl ligands but generally fit into the 13–25 kcal mol^{-1} range. The principal exceptions to this limit are SbCl and $SbCl_5$ whose binding energies border on 30 kcal mol^{-1}. The A···N distances are noticeably longer than the sum of covalent radii, with a ratio tending toward 1.2, considerably larger than the A–Cl ratio which is very close to unity. The AIM quantities are indicative of strong noncovalent bonds, with a certain degree of covalency. The total energy densities of the bond critical points are slightly negative, perhaps −0.01 a.u., and the densities at these same points span a range between 0.03 and 0.07 a.u.

Most of these markers are enhanced upon replacement of the p-block atoms with transition metals of the same row of the periodic table. Binding and interaction energies are elevated up to the 20–55 kcal mol^{-1} range. The bond lengths are only slightly longer than the covalent radii sum with ratios of 1.1 or less. The bond critical point densities are larger as well, some as high as 0.10 a.u., and energy densities more negative, in the range between −0.01 and −0.02. But it must be emphasized that there remains a good deal of sensitivity to the particular metal atom and the number of ligands to which it is bonded. Taking Ru as an example, the binding energies of NH_3 to $RuCl_2$ and $RuCl_4$ are respectively 54 and 28 kcal mol^{-1}, and the energy density H of the former is twice that of the latter. There is no universal rule concerning the influence of the number of ligands. While the binding energy of YCl_3 is considerably larger than that for YCl, the opposite pattern of a

decrease is observed on going from NbCl to $NbCl_3$. Because of the high degree of covalency in these bonds, their strength is poorly related to the depth of the σ or π-hole upon the metal atom. For instance, despite a reduction in V_{max} of $PdCl_4$ as compared to $PdCl_2$, both the interaction and binding energies rise as the two extra Cl ligands are added; a similar reversal is observed in the AgCl and $AgCl_3$ pair.

While it is usually taken for granted that the p-block noncovalent bonds are strengthened as one moves down a column of the periodic table, there is no such clear pattern within the d-block, where the trends are far from uniform. On one hand, there are the spodium bonds where the progression down the column from Zn to Cd to Hg leads to a steady and progressive weakening of the bonds to NH_3, precisely counter to the pattern of bond strengthening of the p-block atoms. But the trend changes for other columns. The Fe → Ru → Os progression finds it is Ru that forms the strongest interactions for MCl_2, whereas there is a small but steady increase for the MCl_4 series. In a complete reversal, the Pd atom of the Ni → Pd → Pt series forms the weakest interaction in the MCl_2 set.

A number of these MCl_n systems have one or more multiplet states that are lower in energy than the singlet. The energetics of binding NH_3 alters for higher multiplicities, but not in a consistent manner. The $TcCl_n$ series serves as an example. The binding energy of singlet TcCl with NH_3 is 25 kcal mol^{-1} in its singlet state, which is ramped up to 44 and 39 kcal mol^{-1} in its triplet and quintuplet states, respectively. On the other hand, the binding of $TcCl_3$ is weakened by higher multiplicity, dropping from 54 kcal mol^{-1} as a singlet, down to 30 and 37 kcal mol^{-1} in the two higher multiplicities. The quintuplet of $TcCl_5$ binds more strongly than does the singlet, 39 *vs.* 23 kcal mol^{-1}.

The replacement of Cl ligands by O has different effects depending upon the nature of the central metal atom. While the binding energies of $MoCl_2$ and $MoCl_4$ are 37 and 30 kcal mol^{-1}, respectively, this quantity is amplified for MoO_2 and MoO_3, up to 46 and 59 kcal mol^{-1}. $RuCl_2$, on the other hand, has its bond to NH_3 weakened from 54 to 35 kcal mol^{-1} in RuO_2. RuO_3 is particularly interesting in that it engages in two minimum-energy complexes with NH_3, that differ in their Ru···N separation. But regardless of whether the intermolecular distance is 2.065 or 3.223 Å, the binding energy with NH_3 is substantially reduced when compared to $RuCl_2$. The Pd series follows its own pattern in that the binding energies of PdO_2 and PdO_3 are slightly lower than those for $PdCl_2$ and $PdCl_3$, but that of PdO_4 is reduced by much more.

Although perhaps weaker than many standard covalent bonds, many of the A···N interactions are at least on the cusp of covalency. The normalized bondlengths are only slightly higher than the sum of atomic covalent radii, larger than the normalized A–Cl distances. The bond critical point densities are significantly higher than 0.04 a.u., which is taken by some as the threshold of covalency.[95] Moreover, the pertinent energy densities are clearly negative, another signal of covalent bonding. Nonetheless, all of these bonding parameters are consistently smaller than those of the clearly covalent A–Cl bonds.

As an alternative to a DFT means of evaluating the various bond strengths, which has certain weaknesses, particularly for systems with small gaps between states of different multiplicity,[96] the interaction energies of the d-block complexes were recomputed in the framework of *ab initio* CCSD. Comparison of these values with the M06-2X data in Table S3 (ESI†) indicate that the more complete *ab initio* protocol reduces these interaction energies by a small amount. But most importantly, these reductions are across the board, and the DFT trends remain intact with CCSD. Sim and coworkers have identified possible sources of error in standard DFT approaches that have to do with the choice of density[97–99] that can have an influence on noncovalent interactions such as halogen bonds,[100] so *ab initio* CCSD calculations were also carried out on the main-group interactions. The same mild reduction with CCSD as compared to DFT occurs for the halogen, chalcogen, pnicogen, and tetrel bonds, as is evident in Table S4 (ESI†). The switching out to a different basis set was also tested. Aug-cc-pVTZ represents a different class of basis sets. Like def2-TZVP, it is also triple-ζ but includes a set of diffuse functions as well. As is evident in the last column of Table S3 (ESI†), this basis set modification had essentially no effect on the interaction energies of any of the complexes.

With regard to relativistic effects, Burguera *et al.*[41] have shown that the relativistic pseudopotential contained within the def2-TZVP basis set yields data very close to that achieved with the exact two-component X2C method for relativistic corrections for the Au atom. Failure to explicitly include these corrections changed the interaction energies by only 0.1 kcal mol^{-1} or less. It is hence thought that this basis set with its relativistic pseudopotential is equally reliable for the other 5d metals W–Hg considered here. Another issue that may have conceivably influenced the results is the integration grid. Alteration from the ultrafine (99 590) to superfine (175 974) caused no change in the computed interaction energies.

As noted above, the connection between the interaction energies and the depths of the σ-holes is a tenuous one. Part of the reason for this poor correlation is the inability of the MEP at that one particular point in space to adequately address the entire electrostatic interaction which covers the potential over the full extent of each subunit. There is also a penetration component to the electrostatic interaction which is likely to be substantial in these bonds which are fairly short. In addition to electrostatics as such, there can be a heavy component of polarization which Clark *et al.* point out is not entirely disconnected from the σ-hole concept.[101,102] Also emphasized by these authors is the difficulty in separating polarization from charge transfer, although there have been some attempts in this direction. For example, Thirman *et al.*[103] have demonstrated the important role played by charge transfer in halogen bonding, without which electrostatics and polarization provide incorrect trends in binding strength. These authors explain how a proper explanation of the trends requires all of the above factors as well as dispersion energy. Along these same lines, means have been developed to evaluate the charge transfer between the two subunits in the forward and reverse directions separately[104] which have been used in the past to better understand vibrational frequency shifts. It is also possible to calculate the

polarization energy within each subunit separate from the other,[105] as implemented in a variety of ionic complexes.

There have been a number of works in the recent literature in which transition metal atoms are linked to electron donors *via* spodium, matere, regium, *etc.* bonding.[33,34,40,42,47,54,106–109] The lengths of these bonds tend to be fairly long, longer than most of the optimized distances computed here. It is important to stress, though, that the bulk of these studies have been concerned with crystals. Rather than optimize the intermolecular separations, calculations have been carried out at the geometries found in the crystals themselves. These structures are confined by crystal packing forces, which would easily account for the distances that are longer than might be achieved by a full geometry optimization of just one pair of subunits. Other studies have been concerned with intramolecular interactions of these types. Again, forces external to the bonding *per se* restrict the two atoms of interest from approaching as closely as they might otherwise do, or disturb their preferred mutual orientations.

In short, then, the external restraints of many systems that have been previously studied have obviated the close approach that would be characteristic of a covalent bond. It is easy to see how these bonds, largely covalent in their natural state, take on a weaker and more noncovalent character when stretched well beyond their desired optimized bondlength. Another factor to consider is that a large proportion of previous studies have involved charged states of one or more of the participating subunits. Placing a negative charge on the Lewis acid would obviously weaken its attraction for a nucleophile, even if there was a shallow σ or π-hole on the metal atom, notwithstanding the overall negative charge. Such a situation would lessen the possibility of a strong, short covalent bond in which the parallel neutral acid would naturally participate.

While there may be some relativistic effects that are not fully covered by the pseudopotential of the basis set, there is reason to believe these effects are small, particularly for the fourth row of the periodic table that is at the heart of this work.[41]

There are several previous studies that have a direct bearing on the results presented here. When Hg was placed in a trivalent system, with two Cl atoms as ligands, combined with a closed shell N-heteroatomic ring,[33] its interaction energy with NH_3 was 8–10 kcal mol^{-1}, a bit smaller than the values for $HgCl_2$ and $HgCl_4$ in Table 3. This result suggests a closed–shell ligand weakens the spodium bond to some extent. A CSD survey of tetracoordinated Hg found what appeared to be a borderline of about 2.55 Å[110] between covalent and noncovalent Hg$\cdots$N distances, corresponding closely to the noncovalent distance of 2.615 Å for $HgCl_4$ found here. The $HgCl_2\cdots NH_3$ binding energy of 12.1 kcal mol^{-1} calculated here matches nicely with the same quantity for several O and S bases that range from 10.6 to 11.7 kcal mol^{-1} [111] in the suitably optimized complexes.

Conclusions

The approach of a neutral nucleophile such as NH_3 to a transition metal atom within the context of a neutral molecule tends toward a strong interaction, with a good deal of covalent character. These bonds are generally somewhat stronger than the noncovalent bonds of p-block atoms that have come to be known as halogen, chalcogen, pnicogen, and tetrel bonds. Although the geometries of these complexes tend to align the nucleophile with the σ or π-hole of the metal center, the strength of the bond is not closely related to the depth of this hole. Unlike the standard p-block noncovalent bonds which undergo a strengthening as the atom moves down a column of the periodic table, there is no such clear pattern for the transition metals. Nor is there a simple relationship between the bond strength and the number or type of ligands that are attached to the central metal.

Data availability

The data that support the findings of this study are available in the ESI† of this article.

Conflicts of interest

The author declares no conflict of interest.

Acknowledgements

This material is based upon work supported by the National Science Foundation under grant no. 1954310.

References

1 G. C. Pimentel and A. L. McClellan, *The Hydrogen Bond*, Freeman, San Francisco, 1960.
2 S. N. Vinogradov and R. H. Linnell, *Hydrogen Bonding*, Van Nostrand-Reinhold, New York, 1971.
3 M. D. Joesten and L. J. Schaad, *Hydrogen Bonding*, Marcel Dekker, New York, 1974.
4 E. Arunan, G. R. Desiraju, R. A. Klein, J. Sadlej, S. Scheiner, I. Alkorta, D. C. Clary, R. H. Crabtree, J. J. Dannenberg, P. Hobza, H. G. Kjaergaard, A. C. Legon, B. Mennucci and D. J. Nesbitt, *Pure Appl. Chem.*, 2011, **83**, 1637–1641.
5 *Hydrogen Bonding – New Insights*, ed. S. J. Grabowski, Springer, Dordrecht, Netherlands, 2006.
6 A. Chand, D. K. Sahoo, A. Rana, S. Jena and H. S. Biswal, *Acc. Chem. Res.*, 2020, **53**, 1580–1592.
7 S. Scheiner and L. Wang, *J. Am. Chem. Soc.*, 1993, **115**, 1958–1963.
8 H. S. Biswal and S. Wategaonkar, *J. Chem. Phys.*, 2011, **135**, 134306.
9 J. E. Del Bene, I. Alkorta, G. Sanchez-Sanz and J. Elguero, *J. Phys. Chem. A*, 2011, **115**, 13724–13731.
10 S. Scheiner and J. Lu, *Chem. – Eur. J.*, 2018, **24**, 8167–8177.
11 A. Bauzá, D. Quiñonero, A. Frontera and P. M. Deyà, *Phys. Chem. Chem. Phys.*, 2011, **13**, 20371–20379.
12 W. Dong, Q. Li and S. Scheiner, *Molecules*, 2018, **23**, 1681.

13 A. Bauzá, T. J. Mooibroek and A. Frontera, *Angew. Chem., Int. Ed.*, 2013, **52**, 12317–12321.
14 S. J. Grabowski, *J. Phys. Chem. A*, 2011, **115**, 12340–12347.
15 S. J. Grabowski, *Phys. Chem. Chem. Phys.*, 2014, **16**, 1824–1834.
16 Z. P. Shields, J. S. Murray and P. Politzer, *Int. J. Quantum Chem.*, 2010, **110**, 2823–2832.
17 G. Chalasinski, S. M. Cybulski, M. M. Szczesniak and S. Scheiner, *J. Chem. Phys.*, 1989, **91**, 7809–7817.
18 P. Politzer, J. S. Murray and Z. Peralta-Inga, *Int. J. Quantum Chem.*, 2001, **85**, 676–684.
19 T. Clark, M. Hennemann, J. S. Murray and P. Politzer, *J. Mol. Model.*, 2007, **13**, 291–296.
20 J. S. Murray, P. Lane, T. Clark, K. E. Riley and P. Politzer, *J. Mol. Model.*, 2012, **18**, 541–548.
21 A. Bauzá, R. Ramis and A. Frontera, *J. Phys. Chem. A*, 2014, **118**, 2827–2834.
22 V. d P. N. Nziko and S. Scheiner, *Phys. Chem. Chem. Phys.*, 2016, **18**, 3581–3590.
23 W. Zierkiewicz, M. Michalczyk and S. Scheiner, *Phys. Chem. Chem. Phys.*, 2018, **20**, 4676–4687.
24 S. Scheiner, *J. Phys. Chem. A*, 2021, **125**, 6514–6528.
25 D. Jovanovic, M. Poliyodath Mohanan and S. M. Huber, *Angew. Chem., Int. Ed.*, 2024, **63**, e202404823.
26 Q. Zhang, Y.-Y. Chan, M. Zhang, Y.-Y. Yeung and Z. Ke, *Angew. Chem., Int. Ed.*, 2022, **61**, e202208009.
27 Y. Lu, Q. Liu, Z.-X. Wang and X.-Y. Chen, *Angew. Chem., Int. Ed.*, 2022, **61**, e202116071.
28 R. Hein, A. Docker, J. J. Davis and P. D. Beer, *J. Am. Chem. Soc.*, 2022, **144**, 8827–8836.
29 A. Docker, X. Shang, D. Yuan, H. Kuhn, Z. Zhang, J. J. Davis, P. D. Beer and M. J. Langton, *Angew. Chem., Int. Ed.*, 2021, **60**, 19442–19450.
30 J. Zhang, A. Hao and P. Xing, *Chem. – Eur. J.*, 2024, **30**, e202401004.
31 Z. Wang, Z. Cao, A. Hao and P. Xing, *Chem. Sci.*, 2024, **15**, 6924–6933.
32 T.-N. Streit, R. M. Gomila, R. Sievers, A. Frontera and M. Malischewski, *CrystEngComm*, 2024, **26**, 594–598.
33 R. Tian, Y. Zeng, X. Li and X. Zhang, *New J. Chem.*, 2024, **48**, 6582–6589.
34 R. M. Gomila, E. R. T. Tiekink and A. Frontera, *Inorganics*, 2023, **11**, 468.
35 P. Middya, M. Karmakar, R. M. Gomila, M. G. B. Drew, A. Frontera and S. Chattopadhyay, *New J. Chem.*, 2023, **47**, 9346–9363.
36 Q. Yang, Q. Wu, X. Zhang, X. Yang and Q. Li, *Mol. Phys.*, 2022, **120**, e2102548.
37 M. Jabłoński, *Molecules*, 2021, **26**, 2275.
38 R. Llull, G. Montalbán, I. Vidal, R. M. Gomila, A. Bauzá and A. Frontera, *Phys. Chem. Chem. Phys.*, 2021, **23**, 16888–16896.
39 R. M. Gomila, A. Bauzá, T. J. Mooibroek and A. Frontera, *CrystEngComm*, 2021, **23**, 3084–3093.
40 A. Bauzá, I. Alkorta, J. Elguero, T. J. Mooibroek and A. Frontera, *Angew. Chem., Int. Ed.*, 2020, **59**, 17482–17487.
41 S. Burguera, A. Bauzá and A. Frontera, *Phys. Chem. Chem. Phys.*, 2024, **26**, 16550–16560.
42 J. Yan, Y. Zeng, L. Meng, X. Li and X. Zhang, *Phys. Chem. Chem. Phys.*, 2023, **25**, 29155–29164.
43 J. Li, Q. Feng, C. Wang and Y. Mo, *Phys. Chem. Chem. Phys.*, 2023, **25**, 15371–15381.
44 M. de las Nieves Piña, T. J. Mooibroek, A. Frontera and A. Bauzá, *Phys. Chem. Chem. Phys.*, 2022, **24**, 24983–24991.
45 A. Pizzi, M. Calabrese, A. Daolio, M. Ursini, A. Frontera and G. Resnati, *CrystEngComm*, 2022, **24**, 3846–3851.
46 A. Shan, X. Li, Y. Zeng, L. Meng and X. Zhang, *New J. Chem.*, 2022, **46**, 3315–3324.
47 G. Sánchez-Sanz, C. Trujillo, I. Alkorta and J. Elguero, *ChemPhysChem*, 2020, **21**, 2557–2563.
48 R. Wang, Z. Wang, X. Yu and Q. Li, *ChemPhysChem*, 2020, **21**, 2426–2431.
49 A. Daolio, A. Pizzi, M. Calabrese, G. Terraneo, S. Bordignon, A. Frontera and G. Resnati, *Angew. Chem., Int. Ed.*, 2021, **60**, 20723–20727.
50 M. Calabrese, A. Pizzi, A. Daolio, R. Beccaria, C. Lo Iacono, S. Scheiner and G. Resnati, *Chem. – Eur. J.*, 2024, **30**, e202304240.
51 S. Burguera, R. M. Gomila, A. Bauzá and A. Frontera, *Crystals*, 2023, **13**, 187.
52 S. Burguera, A. K. Sahu, M. J. Chávez Romero, H. S. Biswal and A. Bauzá, *Phys. Chem. Chem. Phys.*, 2024, **26**, 18606–18613.
53 D. Grödler, S. Burguera, A. Frontera and E. Strub, *Chem. – Eur. J.*, 2024, **30**, e202400100.
54 Y. Xu, M. Calabrese, N. Demitri, A. Pizzi, T. Nag, I. Hung, Z. Gan, G. Resnati and D. L. Bryce, *Chem. Commun.*, 2023, **59**, 12609–12612.
55 I. Alkorta, J. Elguero and A. Frontera, *Crystals*, 2020, **10**, 180.
56 A. Bauzá and A. Frontera, *Chem. – Eur. J.*, 2022, **28**, e202201660.
57 M. Michalczyk, W. Zierkiewicz and S. Scheiner, *Phys. Chem. Chem. Phys.*, 2024, **26**, 5836–5847.
58 M. Calabrese, R. M. Gomila, A. Pizzi, A. Frontera and G. Resnati, *Chem. – Eur. J.*, 2023, **29**, e202302176.
59 Y. Zhao and D. G. Truhlar, *Theor. Chem. Acc.*, 2008, **120**, 215–241.
60 F. Weigend and R. Ahlrichs, *Phys. Chem. Chem. Phys.*, 2005, **7**, 3297–3305.
61 F. Weigend, *Phys. Chem. Chem. Phys.*, 2006, **8**, 1057–1065.
62 L. F. Molnar, X. He, B. Wang and K. M. Merz, *J. Chem. Phys.*, 2009, **131**, 065102.
63 M. A. Vincent and I. H. Hillier, *Phys. Chem. Chem. Phys.*, 2011, **13**, 4388–4392.
64 R. Podeszwa and K. Szalewicz, *J. Chem. Phys.*, 2012, **136**, 161102.
65 S. Karthikeyan, V. Ramanathan and B. K. Mishra, *J. Phys. Chem. A*, 2013, **117**, 6687–6694.
66 M. Majumder, B. K. Mishra and N. Sathyamurthy, *Chem. Phys.*, 2013, **557**, 59–65.
67 M. Walker, A. J. A. Harvey, A. Sen and C. E. H. Dessent, *J. Phys. Chem. A*, 2013, **117**, 12590–12600.
68 A. D. Boese, *ChemPhysChem*, 2015, **16**, 978–985.

69 B. S. D. R. Vamhindi and A. Karton, *Chem. Phys.*, 2017, **493**, 12–19.
70 N. Mardirossian and M. Head-Gordon, *J. Chem. Theory Comput.*, 2016, **12**, 4303–4325.
71 M. J. Frisch, G. W. Trucks, H. B. Schlegel, G. E. Scuseria, M. A. Robb, J. R. Cheeseman, G. Scalmani, V. Barone, G. A. Petersson, H. Nakatsuji, X. Li, M. Caricato, A. V. Marenich, J. Bloino, B. G. Janesko, R. Gomperts, B. Mennucci, H. P. Hratchian, J. V. Ortiz, A. F. Izmaylov, J. L. Sonnenberg, D. Williams-Young, F. Ding, F. Lipparini, F. Egidi, J. Goings, B. Peng, A. Petrone, T. Henderson, D. Ranasinghe, V. G. Zakrzewski, J. Gao, N. Rega, G. Zheng, W. Liang, M. Hada, M. Ehara, K. Toyota, R. Fukuda, J. Hasegawa, M. Ishida, T. Nakajima, Y. Honda, O. Kitao, H. Nakai, T. Vreven, K. Throssell, J. A. Montgomery Jr., J. E. Peralta, F. Ogliaro, M. J. Bearpark, J. J. Heyd, E. N. Brothers, K. N. Kudin, V. N. Staroverov, T. A. Keith, R. Kobayashi, J. Normand, K. Raghavachari, A. P. Rendell, J. C. Burant, S. S. Iyengar, J. Tomasi, M. Cossi, J. M. Millam, M. Klene, C. Adamo, R. Cammi, J. W. Ochterski, R. L. Martin, K. Morokuma, O. Farkas, J. B. Foresman and D. J. Fox, Wallingford, CT, 2016.
72 S. F. Boys and F. Bernardi, *Mol. Phys.*, 1970, **19**, 553–566.
73 Z. Latajka and S. Scheiner, *J. Chem. Phys.*, 1987, **87**, 1194–1204.
74 T. Lu and F. Chen, *J. Comput. Chem.*, 2012, **33**, 580–592.
75 R. F. W. Bader, *Atoms in Molecules, A Quantum Theory*, Clarendon Press, Oxford, 1990.
76 T. A. Keith, *TK Gristmill Software*, Overland Park KS, 2013.
77 K. B. Wiberg, *Tetrahedron*, 1968, **24**, 1083–1096.
78 L. K. Harper, A. L. Shoaf and C. A. Bayse, *ChemPhysChem*, 2015, **16**, 3886–3892.
79 Y. Ge, A. Le, G. J. Marquino, P. Q. Nguyen, K. Trujillo, M. Schimelfenig and A. Noble, *ACS Omega*, 2019, **4**, 18809–18819.
80 T. J. Lee and P. R. Taylor, *Int. J. Quantum Chem.*, 1989, **36**, 199–207.
81 T. J. Lee, J. E. Rice, G. E. Scuseria and H. F. Schaefer, *Theor. Chim. Acta*, 1989, **75**, 81–98.
82 P. Pyykkö and M. Atsumi, *Chem. – Eur. J.*, 2009, **15**, 186–197.
83 M. Kaupp, B. Metz and H. Stoll, *Angew. Chem., Int. Ed.*, 2000, **39**, 4607–4609.
84 S. J. Grabowski, *Understanding Hydrogen Bonds. Theoretical and Experimental Views*, Royal Society of Chemistry, Cambridge, UK, 2021.
85 D. F. Mertsalov, R. M. Gomila, V. P. Zaytsev, M. S. Grigoriev, E. V. Nikitina, F. I. Zubkov and A. Frontera, *Crystals*, 2021, **11**, 1406.
86 M. L. Kuznetsov, *Molecules*, 2021, **26**, 2083.
87 E. Espinosa, I. Alkorta, J. Elguero and E. Molins, *J. Chem. Phys.*, 2002, **117**, 5529–5542.
88 E. Espinosa, E. Molins and C. Lecomte, *Chem. Phys. Lett.*, 1998, **285**, 170–173.
89 A. Obeng and J. Autschbach, *J. Chem. Theory Comput.*, 2024, **20**, 4965–4976.
90 W. Jiang, N. J. DeYonker and A. K. Wilson, *J. Chem. Theory Comput.*, 2012, **8**, 460–468.
91 J. Wang, S. Manivasagam and A. K. Wilson, *J. Chem. Theory Comput.*, 2015, **11**, 5865–5872.
92 D. Süß, S. E. Huber and A. Mauracher, *J. Chem. Phys.*, 2020, **152**, 114104.
93 L. Cheng, J. Gauss, B. Ruscic, P. B. Armentrout and J. F. Stanton, *J. Chem. Theory Comput.*, 2017, **13**, 1044–1056.
94 H. Neugebauer, H. T. Vuong, J. L. Weber, R. A. Friesner, J. Shee and A. Hansen, *J. Chem. Theory Comput.*, 2023, **19**, 6208–6225.
95 I. M. Garazade, A. V. Gurbanov, R. M. Gomila, A. Frontera, A. V. M. Nunes, K. T. Mahmudov and A. J. L. Pombeiro, *New J. Chem.*, 2023, **47**, 15856–15861.
96 M. Reiher, O. Salomon and B. Artur Hess, *Theor. Chem. Acc.*, 2001, **107**, 48–55.
97 S. Vuckovic, S. Song, J. Kozlowski, E. Sim and K. Burke, *J. Chem. Theory Comput.*, 2019, **15**, 6636–6646.
98 S. Song, S. Vuckovic, E. Sim and K. Burke, *J. Phys. Chem. Lett.*, 2021, **12**, 800–807.
99 S. Song, S. Vuckovic, E. Sim and K. Burke, *J. Chem. Theory Comput.*, 2022, **18**, 817–827.
100 E. Sim, S. Song, S. Vuckovic and K. Burke, *J. Am. Chem. Soc.*, 2022, **144**, 6625–6639.
101 T. Clark, J. S. Murray and P. Politzer, *Phys. Chem. Chem. Phys.*, 2018, **20**, 30076–30082.
102 T. Clark and A. Heßelmann, *Phys. Chem. Chem. Phys.*, 2018, **20**, 22849–22855.
103 J. Thirman, E. Engelage, S. M. Huber and M. Head-Gordon, *Phys. Chem. Chem. Phys.*, 2018, **20**, 905–915.
104 M. Loipersberger, Y. Mao and M. Head-Gordon, *J. Chem. Theory Comput.*, 2020, **16**, 1073–1089.
105 H. Shen, S. P. Veccham and M. Head-Gordon, *J. Chem. Theory Comput.*, 2023, **19**, 8624–8638.
106 M. Karmakar, R. M. Gomila, A. Frontera and S. Chattopadhyay, *Cryst. Growth Des.*, 2024, **24**, 5990–6000.
107 A. Daolio, A. Pizzi, G. Terraneo, A. Frontera and G. Resnati, *ChemPhysChem*, 2021, **22**, 2281–2285.
108 F. Yashmin, L. J. Mazumder, P. K. Sharma and A. K. Guha, *Phys. Chem. Chem. Phys.*, 2024, **26**, 8115–8124.
109 A. Frontera and A. Bauzá, *Chem. – Eur. J.*, 2018, **24**, 7228–7234.
110 C. S. Onn, A. F. Hill and J. S. Ward, *Chem. Commun.*, 2024, **60**, 2552–2555.
111 T. Xia, D. Li and L. Cheng, *Chem. Phys.*, 2020, **539**, 110978.

